Chinese Chemical Letters 34 (2023) 107295

Contents lists available at ScienceDirect

Chinese Chemical Letters

journal homepage: www.elsevier.com/locate/cclet

Two-dimensional porous Cu-CuO nanosheets: Integration of heterojunction and morphology engineering to achieve high-effective and stable reduction of the aromatic nitro-compounds

Xinran Dong[a], Zexu Fang[a], Ying Gu[a,*], Xiaoguang Zhou[a,*], Chungui Tian[b,*]

[a] College of Chemistry, Chemical Engineering and Resource Utilization, Northeast Forestry University, Harbin 150040, China
[b] Key Laboratory of Functional Inorganic Material Chemistry, Ministry of Education of the People's Republic of China, Heilongjiang University, Harbin 150080, China

ARTICLE INFO

Article history:
Received 29 December 2021
Revised 12 February 2022
Accepted 3 March 2022
Available online 8 March 2022

Keywords:
Cu-CuO heterojunction
Two-dimensional sheets
Porous
Nitro-compounds
Hydrogenation

ABSTRACT

The morphology and heterojunction engineering are effective ways to boost the performance of Cu-based catalysts. Herein, we have reported the designed synthesis of two-dimensional Cu-CuO heterojunction nanosheets (2D Cu-CuO NS) based on 3-aminopropyl-triethoxysilane (APTES, KH550) aided synthetic strategy. The APTES can act as both the ligand and alkali (-OH) source to guide the large-scale synthesis of 2D Cu-based precursor, which can transform into 2D Cu-CuO NS by the controllable post-treatment. The Si species from APTES can protect the particles from the severe aggregation and growth, guaranteeing the formation of 2D sheets composed of small-sized Cu-CuO heterojunction (about 20 nm). The heterojunction interfaces can provide plentiful active sites to boost the catalytic ability. The 2D sheets can provide large accessible surface, being conducive to the contact of the catalyst and reactants. Benefiting from above virtues, the 2D Cu-CuO NS showed the superior catalytic performance for the reduction of a series of nitro compounds, being superior to most reported non-noble metal-based catalysts. Notably, it exhibited good re-cycled performance with no obvious performance degradation after 10 consecutive catalysis. The present study will be promising to promote the application of the Cu-based catalysts, due to its ability to control the morphology and potential for the large-scale synthesis.

The hydrogenation reaction has played an essential role in the sustainable development [1–3]. Typically, the hydrogenation of aromatic nitro compounds (such as 4-nitrophenol, 4-NP) discarded in water has received intensive attention [4,5]. Some nitro compounds have been listed as priority pollutants by the U.S. Environmental Protection Agency (USEPA) [6,7]. Among many treatment methods (adsorption, biological treatment, *etc.*), the chemical reduction by $NaBH_4$ has been promising because it can be carried out at room temperature and easily detect the conversion process [8–10]. The cost-effective catalysts with suitable electron structure is core in the development of this field. The noble metals (Au, Pd, Pt, *etc.*) have been state-of-the-art catalysts for the reduction of nitro compounds due to their suitable d electronic structure, but suffered from the high cost and low reserve [11,12]. The development of low-cost and effective catalysts, therefore, have been the focus in the field [13,14]. The key to advacing the fields is the adjustment of the morphology and electronic structure, aiming to improve the adsorption/desorption kinetics of reactants on the catalysts, and the mass transfer during the reaction.

Copper-based materials are of promising in advanced fields [15,16]. The Cu has same d electronic structure ($d^{10}s^1$) with the precious metals of Au and Ag, and has a lower price. The virtues makes it became "noble metal-like" catalyst in many fields (*e.g.*, CO_2 reduction, oxidation reactions, and catalytic hydrogenation) [17–19]. The materials with abundant active sites, easy access to the reaction reagents, and enhanced mass transfer should be desired for realizing the effective catalysis. The small-sized colloidal Cu particle can expose more surface sites, thus can catalyze the hydrogenation of 4-NP effectively [20]. However, the colloids particles are not easily separated, thus affecting the recycling and reuse. The performance of the porous copper microspheres (PCMs) decreased obviously after three cycles [21]. To improve the recycling ability of the catalysts, the researchers have loaded the Cu particles on the support [22] or coated the Cu_2O by a ZIF-8 shell [23]. However, the strategy can result in the decrease of the catalytic activity and make the preparation more complicated. Fortunately, by construct-

* Corresponding authors.
E-mail addresses: guying@nefu.edu.cn (Y. Gu), zhouxg78@nefu.edu.cn (X. Zhou), tianchungui@hlju.edu.cn (C. Tian).

https://doi.org/10.1016/j.cclet.2022.03.018
1001-8417/

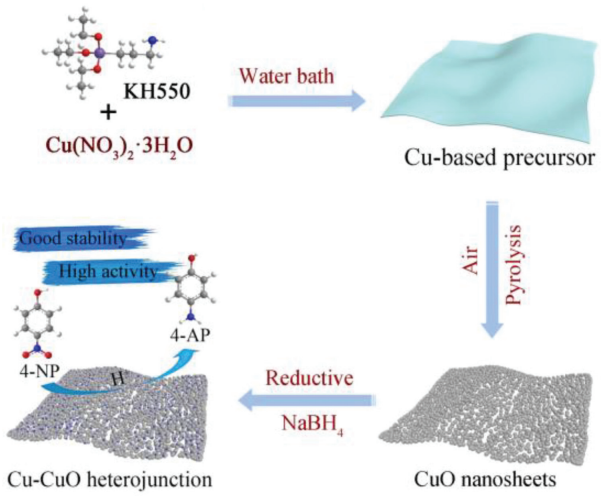

Fig. 1. Schematic illustration of the synthesis process of the 2D Cu-CuO heterojunction nanosheets.

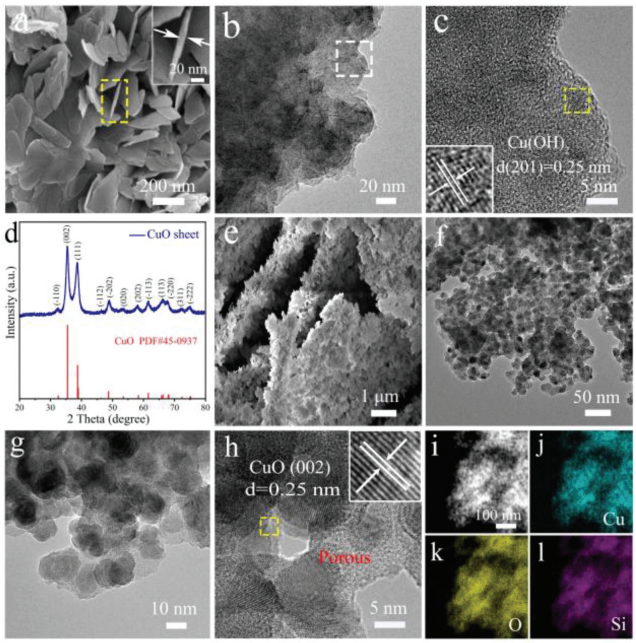

Fig. 2. (a) typical SEM image, (b, c) TEM images (Inset is HRTEM image) of 2D Cu-based precursor; (d) XRD pattern, (e) SEM, (f-h) TEM images, (i) STEM image and (j-l) EDS elemental mapping images of 2D CuO nanosheets.

ing the sphere-like and rod-like assemblies composed of particles [24,25] the separation and reused ability can be improved, showing the large potential of the assembly as effective catalysts. It is well known that 2D materials have large accessible specific surfaces, being favorable for catalytic application [26,27]. Also, the construction of the heterojunction interfaces can make more active sites, thus boosting the catalytic ability [28,29]. The large-scale synthesis is very important for the practical application [30]. Therefore, it is desired to design of 2D Cu-based heterojunction with high output for the effectively catalytic application.

The reaction of Cu salts with the alkaline ($NH_3{\cdot}H_2O$, NaOH, *etc.*) in the presence of additives (surfactant, *etc.*) are general ways to prepare the Cu-based materials with well-defined morphology and size [31,32]. The 3-aminopropyl-triethoxysilane (APTES, KH550) containing the amino groups (can combine with metal ions) and Si species is a kind of excellent coupling agent [33,34]. Herein, the synthesis of the 2D Cu-CuO heterojunction nanosheets (2D Cu-CuO NS) were shown based on APTES-aided synthetic strategy. The APTES can act as both the ligand and alkali source (-OH) to guide the large-scale synthesis of 2D precursor sheets (above 10 g for one time of the synthesis), which can transform into 2D Cu-CuO NS by the controllable treatment. The Si species from APTES can protect the particles from severe aggregation and growth during the synthesis, guaranteeing the formation of the 2D sheets composed of small-sized Cu-CuO heterojunction. Benefiting from the special structure, the 2D Cu-CuO NS showed superior catalytic performance for the reduction of various aromatic nitro-compounds, being superior to the most reported non-noble metal-based catalysts. Moreover, it exhibited good re-cycled performance with no obvious performance degradation after 10 consecutive catalytic benefited from the 2D assembled structure.

The synthesis of 2D Cu-CuO heterojunction nanosheets was schematically illustrated in Fig. 1. The silane coupling agent (KH550), which can act as the coordination agent and alkaline source, was selected for the reaction with Cu ion to form the precursor nanosheets. The reaction of $Cu(NO_3)_2{\cdot}3H_2O$ and KH550 solution can give the 2D Cu-based precursor sheets with high yield (reaching 10 g for each time synthesis and can be easily scaled-up) (Fig. S1 in Supporting information). The 2D Cu-based precursor can transform into 2D CuO NS by the controllable post-treatment. Finally, the 2D Cu-CuO heterojunction was formed by reduction of CuO NS with $NaBH_4$.

The morphology and composition of the Cu-based precursors were characterized by XRD, SEM and TEM. In the XRD pattern of Cu-based precursors (Fig. S2 in Supporting information), the diffraction peaks at 13.3°, 26.9° and 35.9° can be indexed to the (001), (002) and (201) planes of orthorhombic $Cu(OH)_2$ (PDF #42–0638) [35]. The -OH should be from the hydrolysis of KH550 in the synthesis. The SEM image (Fig. 2a) shows the uniform sheets. An enlarged image shows that the diameter of the sheets is about 200 nm with thickness below 10 nm. The TEM images (Figs. 2b and c) further verify the formation of thin nanosheets. The plane distance of 0.25 nm corresponds to the (201) plane of $Cu(OH)_2$. The sheet-like Cu-based materials provided ideal precursors for the preparation of 2D Cu-based catalysts. The energy-dispersive X-ray spectroscopy (EDS) element mapping images reveal the homogeneous distribution of Cu, O and Si elements in the precursor sheet (Fig. S3 in Supporting information), in which the Si elements (about 5% in mass) should be come from KH550 coordinated with Cu^{2+}. The formation of 2D Cu-based precursor sheets can be related to the specificity of KH550. The KH550 can combine with the Cu^{2+} ions based on the coordination of -NH_2 with metal ions [36]. Also, the KH550 can hydrolyze slowly in the $Cu(NO_3)_2{\cdot}3H_2O$ solution to release the -OH (pH ~9). The formed -OH can combine with Cu^{2+} to generate $Cu(OH)_2$. The coordination of KH550 with the Cu^{2+} can induce the formation of sheet-like structure [34]. The synergistic coordination of -OH and KH550 with Cu^{2+} can produce the 2D Cu-based precursor sheets. The synthesis process is very simple and the yield is high (above 10 g for each time synthesis). The theoretical yield is about 4.9 g if all the Cu^{2+} (0.05 mol) was transformed into $Cu(OH)_2$, while the theoretical yield is about 20 g if all Cu^{2+} (0.05 mol) was combined with KH550 (KH550-Cu). The yield of Cu-based precursor (10 g) is much higher than 4.9 g, so the 2D precursor is formed by the combination of Cu^{2+} with -OH and KH550.

The CuO is a useful catalyst for many catalytic reactions such as methanol oxidation [37] and reduction [38], but the CuO previously reported still has disadvantages such as large particle size, and low yields. The Cu-based sheet-like precursors provide a platform for the synthesis of CuO. To this, the precursor is heated

in air to obtain CuO. In the pyrolysis process, the CuO can be formed by the reaction of oxygen with Cu^{2+} in the air and dehydration of $Cu(OH)_2$ in the precursor. The dehydration and decomposition of organic components can make the formation of porous structures. The crystal structure of the CuO NS was determined with XRD, as shown in Fig. 2d. The peaks located at 35.55°, 38.67° and 48.84° are assigned to the (002), (111) and ($\bar{2}$02) planes of monoclinic CuO (PDF #45–0937). The broad diffraction peaks imply the small crystalline size of CuO. The SEM image reveals the recombination of the nanosheet precursors during pyrolysis and form CuO nanosheets with larger sizes than the 2D Cu-based precursor (Fig. 2e). Furthermore, TEM images (Figs. 2f and g) clearly indicate the thin CuO nanosheet composed uniform nanoparticles with a diameter of about 10 nm. There are abundant pores between the particles that make up the nanosheet. The high-resolution TEM (HRTEM) image (Fig. 2h) clearly shows the lattice fringes of 0.25 nm, which can be indexed to the (002) crystal plane of CuO. The Si species from KH550 can protect the particles from severe growth and agglomeration, thus forming the sheets composed of small CuO particles. The elemental mapping confirms the uniform distribution of Cu, O and Si elements throughout the sheet (Figs. 2i-l). In summary, porous CuO nanosheets composed of small nanoparticles were obtained by pyrolysis of the Cu-based nanosheet precursors in air atmosphere.

There are some reports about the use of CuO as the catalysts for the catalytic reduction of aromatic nitro compounds. In view of the advantage of the 2D porous structure, the catalytic performance of the 2D porous CuO nanosheets was first evaluated by using the reduction of 4-NP into 4-AP in the presence of $NaBH_4$. The test shows that the reaction can be completed within about 390 s (Fig. S4a in Supporting information). Surprisingly, during the reused cycle, the catalyst showed significantly improved performance. It takes only about 155 s to completely reduce 4-NP at the same concentration (Figs. S4b and c in Supporting information). We speculate that CuO is partially reduced to Cu due to the reduced ability of $NaBH_4$, thus forming Cu-CuO heterojunction. It can be demonstrated by the XRD pattern (Fig. S5 in Supporting information). The heterojunction catalysts can accelerate the charge transfer and produce an interface favorable to the adsorption/activation of active species, being favorable for the catalytic reaction [39,40]. Therefore, we have purposefully treated the CuO sheets with $NaBH_4$ to obtain Cu-CuO heterojunction. The XRD of the samples after being treated with $NaBH_4$ shows the peaks belonging to CuO and Cu (Fig. 3a). The crystalline peaks located at 43.29°, 50.43° and 74.17° are corresponded to (111), (200) and (220) planes of cubic copper (PDF #04–0836). The SEM image in Fig. 3b shows that the Cu-CuO sample shows still a sheet-like structure. Furthermore, the TEM images (Figs. 3c and d) clearly indicates the porous structure of Cu-CuO sheets composed of small particles with a diameter of about 10 nm. The HRTEM (Fig. 3e) image discloses the two adjacent lattice spacing of 0.21 and 0.23 nm, which are indexed to (111) and (111) plane of the Cu and CuO, respectively. The interfaces between Cu and CuO can be observed. The STEM image and elemental mapping (Figs. 3f-i) show the homogeneous distribution of Cu, O and Si throughout the nanosheet. All characterization indicates the formation of 2D Cu-CuO porous sheets.

X-ray photoelectron spectroscopy (XPS) is performed to determine the elementary composition and valence states of the samples. The survey spectra show (Fig. 4a and Fig. S6 in Supporting information) the existence of C, Si, O and Cu elements in the three samples. In the Cu 2p of Cu-based precursor (Fig. S7a in Supporting information), the two characteristic peaks at 954.4 and 934.4 eV are assigned to Cu $2p_{1/2}$ and Cu $2p_{3/2}$, which are consistent with the characteristics of Cu^{2+} in $Cu(OH)_2$ [41]. The remaining two peaks at 942.6 and 962.3 eV are satellite peaks of Cu^{2+}. The Si 2p

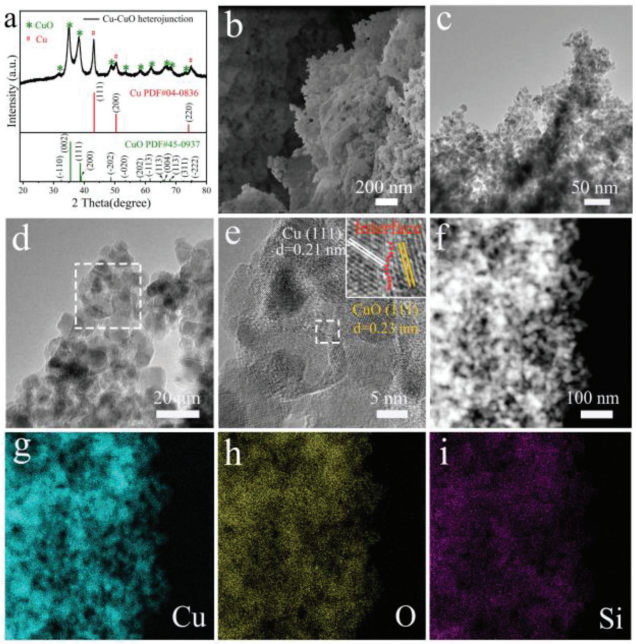

Fig. 3. (a) XRD pattern, (b) typical SEM image, (c, d) TEM images, (e) HRTEM image, (f) STEM and (g-i) EDS elemental mapping images of 2D Cu-CuO heterojunction.

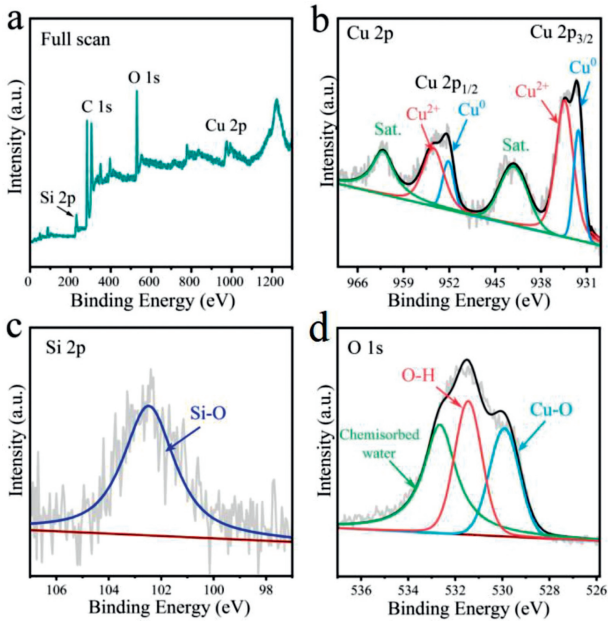

Fig. 4. XPS spectra of Cu-CuO NS in the (a) survey spectra (b) Cu 2p, (c) Si 2p and (d) O 1s, respectively.

XPS spectrum in Fig. S8 shows typical Si-O peak at 101.6 eV, which is attributed to the O-Si bond from Si species [42]. The XPS results are consistent with those obtained by XRD and TEM. The combination of XPS with TEM and XRD further supports the formation of $Cu(OH)_2$ nanosheet containing Si species. For the CuO nanosheet, the peaks at 934.3 and 954.3 eV are ascribed to Cu $2p_{3/2}$ and Cu $2p_{1/2}$ for CuO (Fig. S7b in Supporting information) [43]. In the Cu 2p high-resolution XPS spectrum (Fig. 4b) of Cu-CuO samples, the characteristic peaks at 934.1 eV and 954.1 eV of Cu^{2+} are indexed to CuO, and the characteristic peak at 932.2 and 952.0 eV are assigned to Cu^0 from Cu [44]. The result further demonstrates the formation of Cu-CuO heterojunction. The Si 2p spectrum in Fig. 4c exhibits the fitting peak at 102.5 eV, which is attributed to the O–

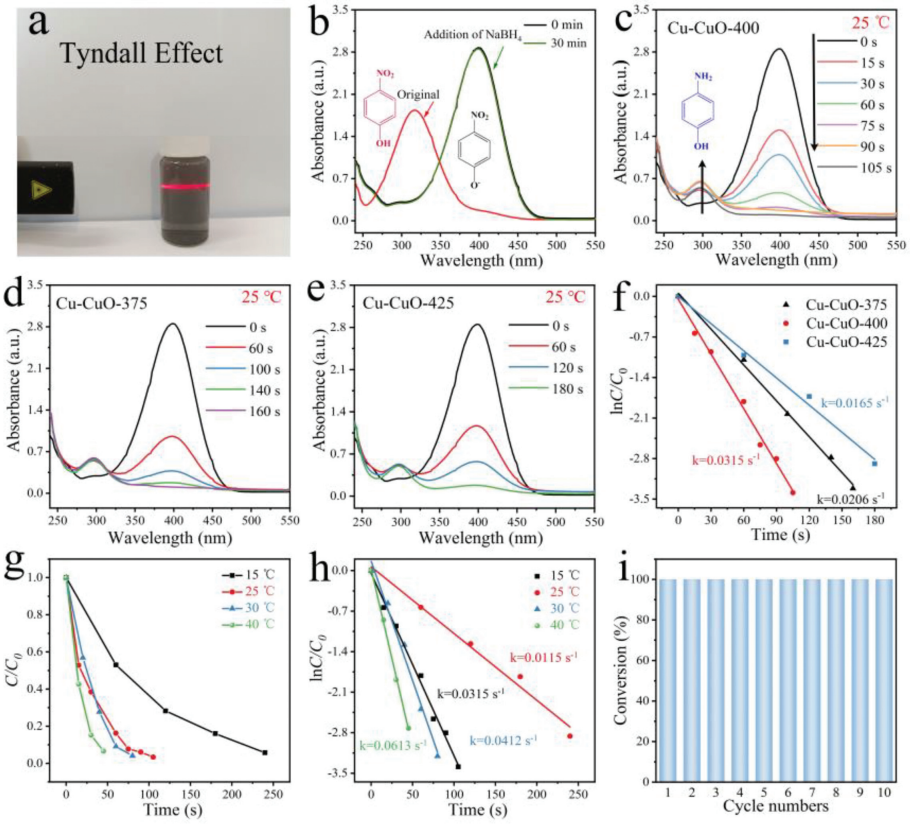

Fig. 5. (a) The photo shows the well dispersion of Cu-CuO-400 sheets in aqueous solution. (b) UV–vis spectra of 4-NP solution before and after addition of $NaBH_4$. Time-dependent UV–vis spectra of 4-NP reduction over (c) Cu-CuO-400 heterojunction, (d) Cu-CuO-375 and (e) Cu-CuO-425; (f) Plot of $\ln(C/C_0)$ *versus* reaction time for the reduction of 4-NP over different catalysts at 25 °C. (g) Variation of C/C_0 *versus* reaction time and (h) plot of $\ln(C/C_0)$ *versus* reaction time for the reduction of 4-NP by Cu-CuO-400 sheets at different temperatures. (i) Repeated catalytic tests of Cu-CuO-400 catalyst.

Si bond from Si species [42]. The formation of this Si-O species has a good protective effect on the sheet during the pyrolysis and reduction, so that the porous sheets composed of small particles can be formed [45]. From Fig. 4d, the O 1s XPS spectrum of Cu-CuO heterojunction shows three peaks at 529.9, 531.5 and 532.6 eV arising from metal-O, chemically adsorbed hydroxyl oxygen, and adsorbed water molecules [46]. Compared with CuO samples, the shift of Cu^{2+} peak position (0.2 eV) to low binding energy in Cu-CuO samples proves that the existence of strong electronic interaction between Cu and CuO, which is favorable to improve the catalytic performance [47]. The results of XRD, TEM and XPS convincingly suggest that the porous Cu-CuO heterojunction nanosheets are successfully synthesized.

As a refractory organic contaminant discharged into the aquatic system by pesticide and petrochemical industry, *p*-NP has given rise to significant public health and environmental risk in humans and aquatic organisms. However, the reduction product *p*-AP is less toxic than *p*-NP. It is a primary raw material for many analgesic and antipyretic drugs. Thus, the reduction of *p*-NP to *p*-AP can not only eliminate pollutants to protect the environment, but also realize waste utilization in industrial production. In this regard, the reduction of 4-NP into 4-AP is used as a model for evaluating the catalytic efficiency of the Cu-based catalysts. The reduction process was monitored by UV–vis spectroscopy. The well-dispersion is conducive to the contact of the catalyst and the reactant, which can promote the catalytic reaction of the catalyst. As shown in Fig. 5a, the Cu-CuO sheet can be uniformly dispersed in aqueous solutions and shows an obvious Tyndall effect, which is conducive to developing its performance. As shown in Fig. 5b, the solution of 4-NP exhibits a strong absorption peak at 319 nm, which was red-shifted to 400 nm with the addition of $NaBH_4$ due to the deprotonation of 4-NP. Correspondingly, a color change from pale yellow to bright yellow was observed. After standing 30 min, no further change was observed, implying that the hydrogenation reaction could not happen in the sole presence of $NaBH_4$. Fig. 5c shows the time-dependent UV–vis absorption spectra recorded during the 4-NP reduction catalyzed by Cu-CuO heterojunction, in which the absorption peak at 400 nm significantly decreases within 105 s. However, it takes 30 min and 390 s over Cu-based precursor (Fig. S9 in Supporting information) and CuO catalyst, respectively. The results show that the construction of Cu and CuO heterogeneous interfaces can significantly improve the catalytic activity.

The catalytic activity of the other two catalysts (Cu-CuO-375 and Cu-CuO-425) for 4-NP reduction were also evaluated as illustrated in Figs. 5d and e. It takes 160 s and 180 s for Cu-CuO-375 and Cu-CuO-425 catalysts to almost completely convert 4-NP to 4-AP, respectively. Combined with the XRD spectra (Fig. S10 in Supporting information) and SEM images (Fig. S11 in Supporting information), it can be shown that the samples from low pyrolysis temperature have low crystallinity, which can result in low catalytic activity. However, the high pyrolysis temperature is not conducive to the preservation of sheet morphology in the calcination process, so the catalytic performance also decreases. The amount of $NaBH_4$ obviously exceeds that of 4-NP, and the reduction rate can be considered to be roughly independen of the concentration of $NaBH_4$. The reaction kinetic was considered as a quasi-first-order kinetic reaction only of 4-NP. The linear relationships of C/C_0 and $\ln(C/C_0)$ *versus* reaction time are obtained over the three catalysts (Fig. S12 in Supporting information and Fig. 5f). Correspondingly, the apparent rate constant k_{app} of Cu-CuO-400 (0.0315 s^{-1}) was higher

Table 1
Catalytic reduction of several nitro compounds over Cu-CuO heterojunction.

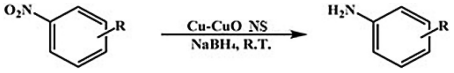

Substrate	Product	Time (s)	Substrate	Product	Time (s)
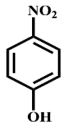	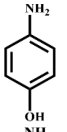	105	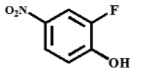	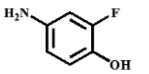	45
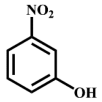	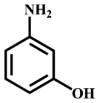	7	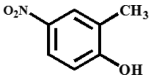	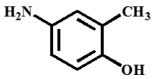	90
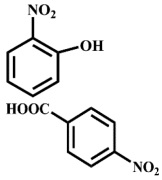	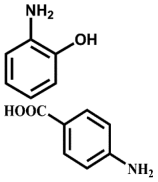	36	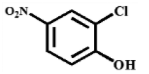	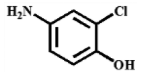	42
		10	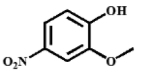	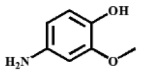	240

Reaction conditions: substrate (0.2 mmol/L), V (30 mL), $NaBH_4$ (10 mg), catalyst (5 mg). The solvent is distilled water or a mixed solution of distilled water and ethanol. Determined by UV–vis spectrum.

than that of Cu-CuO-375 (0.0206 s^{-1}) and Cu-CuO-425 (0.0165 s^{-1}), further validating the highest catalytic efficiency of Cu-CuO-400. The optimum activity (Fig. S13 in Supporting information) was obtained when the mass ratio of sodium borohydride to CuO was 2:1. In particular, the catalytic reduction activity of Cu-CuO heterojunction is also higher than that of some reported Cu-based catalysts, and even higher than that of some noble metal-based catalysts (Table S2 in Supporting information).

The dependence of the catalytic activity of Cu-CuO heterojunction on reaction temperature was also investigated, and the UV–vis spectra are shown in Fig. S14 (Supporting information). Figs. 5g and h show the C_t/C_0 and $\ln(C_t/C_0)$ *versus* reaction time of the Cu-CuO heterojunction catalysts at different reaction temperatures (15, 25, 30 and 40 °C). The results show that in the presence of Cu-CuO heterojunction catalyst, the reduction rate of 4-NP by $NaBH_4$ increases with the increase of reaction temperature. This observation can be explained by collision theory [48]. The particles may react during the collision. As the temperature of the system increases, the violent motion of the particles will increase the chance of collisions, which results in the faster reactions rate. The apparent activation energy of the catalytic reaction was calculated according to the Arrhenius equations (Eqs. 1 and 2):

$$k = Ae^{-\left(\frac{E_a}{RT}\right)} \quad (1)$$

$$\ln k = \ln A - \frac{E_a}{RT} \quad (2)$$

where k is the rate constant, A is the pre-exponential factor, E_a is the activation energy, R is the gas constant (8.314 J mol^{-1} K^{-1}), and T is the temperature. The apparent activation energy of the catalytic reaction calculated according to the Arrhenius equation is 51.15 kJ/mol.

In addition to the performance, the cycle stability of the catalyst is also a very important factor for the application. As shown in Fig. 5i, Cu-CuO catalyst still maintains a catalytic efficiency of more than 99% after 10 times of cycles, which is superior to many reported catalysts. The Cu-CuO samples after catalytic reduction of 4-NP were also characterized. As shown in Fig. S15 (Supporting information), the diffraction peaks of the sample after catalytic hydrogenation of 4-NP is similar to that of the original Cu-CuO heterojunction catalysts, implying the good stability of the catalyst. Moreover, the TEM and STEM image (Fig. S16 in Supporting information) shows that there is no obvious change in the morphology of the Cu-CuO heterojunction catalysts after the catalytic reaction, suggesting good structural stability of the catalysts. Above results verify the good catalytic activity and stability of Cu-CuO catalyst, which is very favorable for practical application.

Besides 4-NP, there are many aromatic amines, which are important intermediates in the preparation of several nitrogen-containing biologically active compounds, agrochemicals, pharmaceuticals, *etc*. Therefore, it is particularly important to prepare non-noble metal catalysts with high efficiency for the reduction of various aromatic nitro compounds. As shown in Table 1, Figs. S17 and S18 (Supporting information), Cu-CuO heterojunction catalyst only needs 36 and 7 s to reduce *o*-nitrophenol and *m*-nitrophenol to form corresponding aminobenzene. Some complex nitrobenzene containing more functional groups can also be reduced to corresponding aminobenzene within a short time. So, the prepared porous Cu-CuO heterojunction catalysts have excellent catalytic hydrogenation activity for many aromatic compounds, which is beneficial to their practical application.

The possible catalytic mechanism for the reduction of 4-NP to 4-AP by the Cu-CuO heterojunction catalyst is shown in Fig. 6. First of all, 4-NP ions and BH_4^- ions are reversibly adsorbed on the surface of Cu-CuO catalysts [49]. BH_4^- ion reacts with H_2O to form BO_2^- and H while the resulting H will immediately combine with the catalyst to form the adsorbed metal-H species [50,51]. Afterwards, these dissociative hydrogen species react with 4-NP molecules to form nitroso-compound and hydroxyamino-compound. Finally, the hydroxyamino compound is reduced to the final product 4-AP. Finally, the formed 4-AP molecule is desorbed spontaneously from the surface of the Cu-CuO catalyst. The catalytic activity of Cu-CuO heterojunction nanosheets is better than that of pure CuO, which indicates that the construction of heterogeneous can provide more active interfaces for active BH_4^- to form H atoms and transfer electrons rapidly. By combining a series of experimental and characterization results, the excellent performance of Cu-CuO catalysts should be ascribed to synergy between Cu and CuO for adjusting the electronic structure and facilitating the adsorption/desorption of intermediates on the catalyst. In addition, the large reachable surface provided by the 2D sheet and abundant pore structures on the sheet facilitate mass

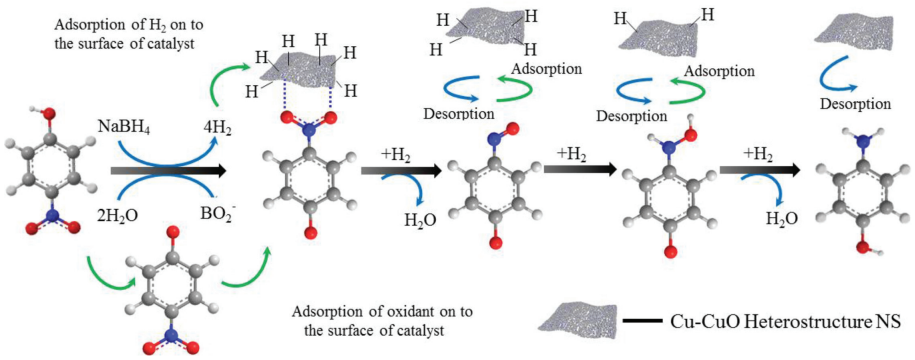

Fig. 6. Illustrative catalytic mechanism for 4-NP reduction to 4-AP by heterojunction.

transfer promotes the contact of the catalyst and reactants. Benefiting from above virtues, the 2D Cu-CuO NS showed the superior catalytic performance for the reduction of a series of nitro compounds, being superior to most reported non-noble metal-based catalysts. Notably, it exhibited good re-cycled performance with no obvious performance degradation after 10 consecutive catalysis. In addition, the Si species from APTES can protect the particles from severe aggregation and growth during the synthesis, but also contribute to the stability of catalyst during the catalytic transformation process.

In summary, we have demonstrated a new method for the synthesis of high-effective 2D porous Cu-CuO heterojunction catalyst. The key for the designed synthesis is the use of the KH550 that can act as alkaline ligands and coordination agents to induce the formation of the 2D Cu-based precursor with high yields, which can be subsequently converted into the 2D porous Cu-CuO heterojunction. The 2D heterojunction exhibits an excellent catalytic activity and stability for the reduction of the aromatic nitro-compounds, being at the forefront of reported non-noble metal catalysts. The good performance is related to the 2D sheets for providing large accessible surfaces, the abundant pores beneficial for mass transfer, and the heterogeneous interface for providing more active sites. This work would be promising for the practical application of the Cu-based catalysts benefited from the easy, high-yielded synthesis and special 2D, porous heterojuction structure for effective catalysis.

Declaration of competing interest

The authors declare that we have no known competing financial interests or personal relationships that could have appeared to influence the work reported in this paper.

Acknowledgments

We gratefully acknowledge the support of this research by the National Natural Science Foundation of China (No. 91961111), the Natural Science Foundation of Heilongjiang Province (No. ZD2021B003).

Supplementary materials

Supplementary material associated with this article can be found, in the online version, at doi:10.1016/j.cclet.2022.03.018.

References

[1] K. Murugesan, T. Senthamarai, V.G. Chandrashekhar, et al., Chem. Soc. Rev. 49 (2020) 6273–6328.
[2] N. Garg, A. Sarkar, B. Sundararaju, Coord. Chem. Rev. 433 (2021) 213728.
[3] Y. Wang, E. Luo, X. Wang, et al., Chin. Chem. Lett. 32 (2021) 506–510.
[4] L. Zhang, M. Zhou, A. Wang, et al., Chem. Rev. 120 (2019) 683–733.
[5] F. Mo, D. Qiu, L. Zhang, et al., Chem. Rev. 121 (2021) 5741–5829.
[6] Q. Liu, T. Xu, Y. Luo, et al., Curr. Opin. Electrochem. 29 (2021) 100766.
[7] Y. Wang, R. Qin, Y. Wang, et al., Angew. Chem. Int. Ed. 59 (2020) 12736–12740.
[8] Y. Xu, X. Shi, R. Hua, et al., Appl. Catal. B 260 (2020) 118142.
[9] Z. Yan, X. Xie, Q. Song, et al., Green Chem. 22 (2020) 1301–1307.
[10] T.B. Nguyen, C. Huang, R.A. Doong, Appl. Catal. B 240 (2019) 337–347.
[11] L. Zhang, J. Liang, Y. Wang, et al., Angew. Chem. Int. Ed. 60 (2021) 25263–25268.
[12] Y. Luo, S. Fan, W. Yu, et al., Adv. Mater. 30 (2018) 1704576.
[13] K.Zhao X.S, C. Wang, et al., Chin. Chem. Lett. 32 (2021) 2963–2974.
[14] Z. Li, Z. Ma, J. Liang, et al., Mater. Today Phys. 22 (2022) 100586.
[15] M.B. Gawande, A. Goswami, F.X. Felpin, et al., Chem. Rev. 116 (2016) 3722–3811.
[16] B. Yang, X. Yu, A. Halder, et al., ACS Sustain. Chem. Eng. 7 (2019) 14435–14442.
[17] D. Karapinar, C.E. Creissen, J.G. Rivera de la Cruz, et al., ACS Energy Lett. 6 (2021) 694–706.
[18] L. Sun, Y. Wang, C. Wang, et al., Chem 7 (2021) 1557–1568.
[19] L. Jin, G. He, J. Xue, et al., J. Cleaner Prod. 161 (2017) 655–662.
[20] W. Tan, N.A. Bakar, M.A. Bakar, Catal. Lett. 145 (2015) 1626–1633.
[21] M. Li, Y. Su, J. Hu, et al., Mater. Res. Bull. 83 (2016) 329–335.
[22] A. Taghizadeh, K. Rad-Moghadam, J. Cleaner Prod. 198 (2018) 1105–1119.
[23] B. Li, J.G. Ma, P. Cheng, Angew. Chem. 130 (2018) 6950–6953.
[24] A. Zhang, L.Xue J.Wu, et al., ACS Appl. Mater. Interfaces 13 (2021) 46577–46587.
[25] D. Yin, G. Huang, Z. Na, et al., ACS Energy Lett. 2 (2017) 1564–1570.
[26] S. Wan, J. Wu, D. Wang, et al., Chin. Chem. Lett. 32 (2021) 816–821.
[27] X. Zhang, T. Wu, H. Wang, et al., ACS Catal. 9 (2019) 4609–4615.
[28] G. Yang, Y. Jiao, H. Yan, et al., Adv. Mater. 32 (2020) 2000455.
[29] Y. Gu, A. Wu, Y. Jiao, et al., Angew. Chem. 133 (2021) 6747–6755.
[30] Y. Gu, Y. Jiao, X. Zhou, et al., Nano Res. 11 (2017) 126–141.
[31] X. He, Y. Wang, X. Zhang, et al., ACS Catal. 9 (2019) 2213–2221.
[32] Y. Dai, F. Li, D.C. Mo, et al., ACS Appl. Mater. Interfaces 13 (2021) 26404–26410.
[33] Y. Liu, J. Yin, Y. Fu, et al., Chem. Eng. J. 382 (2020) 122925.
[34] J. Zhao, Y. Niu, B. Ren, et al., Chem. Eng. J. 347 (2018) 574–584.
[35] Q. Li, W. Deng, C. Li, et al., ACS Appl. Mater. Interfaces 10 (2018) 40265–40273.
[36] S. Lu, L. Xia, J. Xu, et al., ACS Appl. Mater. Interfaces 11 (2019) 18626–18636.
[37] M. Huang, W. Xiang, C. Wang, et al., Chin. Chem. Lett. 31 (2020) 2769–2773.
[38] S. Singh, N. Kumar, M. Kumar, et al., Chem. Eng. J. 313 (2017) 283–292.
[39] G. Wen, J. Liang, Q. Liu, et al., Nano Res. 15 (2022) 972–977.
[40] T. Xu, J. Liang, Y. Wang, et al., Nano Res. 15 (2022) 1039–1046.
[41] J.Q. Xie, Y.Q. Ji, J.H. Kang, et al., Energy Environ. Sci. 12 (2019) 194–205.
[42] S.H. Joo, J.Y. Park, C.K. Tsung, et al., Nat. Mater. 8 (2009) 126–131.
[43] Q. Chang, W. Xu, N. Li, et al., Appl. Catal. B 263 (2020) 118299.
[44] C. Zhang, W. Lv, G. Zhou, et al., Adv. Energy Mater. 8 (2018) 1703404.
[45] X. Zhang, Y. Zhao, X. Jia, et al., Adv. Energy Mater. 8 (2018) 1702780.
[46] H.S. Mohamed, C.F. Li, L. Wu, et al., Chem. Eng. J. 407 (2021) 126941.
[47] A. Wu, Y. Gu, B. Yang, et al., J. Mater. Chem. A 8 (2020) 22938–22946.
[48] Z. Wang, R. Su, D. Wang, et al., Ind. Eng. Chem. Res. 56 (2017) 13610–13617.
[49] J. Li, L. Zhong, L. Tong, et al., Adv. Funct. Mater. 29 (2019) 1905423.
[50] J. Pritchard, G.A. Filonenko, R. Van Putten, et al., Chem. Soc. Rev. 44 (2015) 3808–3833.
[51] F. Wang, S. Song, K. Li, et al., Adv. Mater. 28 (2016) 10679–10683.